ELSEVIER

Chemical Engineering Journal 140 (2008) 358–369

Chemical Engineering Journal

www.elsevier.com/locate/cej

Prediction of bubble behaviour in fluidised beds based on solid motion and flow structure

Xianfeng Fan [a,*], Zhufang Yang [a,b], David J. Parker [a], Brian Armstrong [b]

[a] *School of Physics and Astronomy, University of Birmingham, Birmingham B15 2TT, UK*

[b] *Department of Chemical Engineering, School of Engineering, University of Birmingham, Birmingham B15 2TT, UK*

Received 20 May 2007; received in revised form 10 October 2007; accepted 12 October 2007

Abstract

It has been demonstrated that the non-intrusive positron emission particle tracking (PEPT) could be a potential technique for observing bubble flow pattern, measuring bubble size and rise velocity in bubbling fluidised beds according to the solid motion in bubble and its wake. The results indicate that the behaviour of air bubbles varies greatly with the bed materials and superficial gas velocity. Three types of bubbling patterns (namely A, B and C) have been reported in this study, in which the pattern C is observed when the polyethylene fluidised bed is operated at the superficial gas velocity ($U - U_{mf}$) of 0.25–0.5 m/s and the ratio of bed height to bed diameter is unity. After the comparison of the results measured by the PEPT technique with the values calculated by using a number of empirical correlations, two modified correlations are recommended to calculate the bubble size based on the PEPT data.

Keywords: Fluidisation; Bubble size; Bubble velocity; Bubbling pattern; Flow structure

1. Introduction

Bubbling fluidisation has been seen as an effective means for providing good mixing and contact of gas and solid phases, as well as providing good heat transfer [1–3]. These attractive features are achieved by injection of air to create a bubble flow via a perforated or porous surface through the solid beds. The fluidisation quality of a bed is, therefore, highly dependent on bubble distribution and bubble physical properties in a bed. Ideally, for there to be good quality fluidisation the population of bubbles in a bed should be large, but the bubbles should be small in size, and homogeneously occupy the bed [4–8].

Despite the extensive work carried out since 1960s, questions still remain. Grace and Harrison [9] were among the first to systematically and quantitatively investigate the spatial distribution of bubbles in a two-dimensional bed by means of photography. They suggested that the bubbles with small sizes were uniformly distributed in a layer close to the distributor and then shafted inwards to the central region of the bed with the increase in the bed height, resulting in the reduction in concentration of bubbles in the region near the walls. This was used as a basis by Darton et al. [10] for the popular model of bubble coalescence. However, a different observation was reported by Werther and Molerus [11,12] when they investigated the bubble spatial distribution in three-dimensional beds containing quartz sand, glass spheres and spherical copper powder under various operating conditions by using capacitance probes. Close to the distributor air bubbles preferentially formed in the vicinity of the walls, rather than being uniformly distributed in the whole cross-section area. As the bubbles rose in the bed, the diameter of this annulus of bubbles decreased until a single peak formed at the centre of a bed. The packing geometry of the particle layers near the wall was altered, as in packed beds and liquid-fluidised beds, therefore, leading to an increased flow through this region. In experiments recently carried out by Lim et al. [8] in a planar fluidised bed, the bubble void fraction (BVF) was calculated by real-time vision instrumentation which accumulated images over time. The reported bubble distribution was similar to Werther and Molerus [11,12] wherein a pair of narrow bands of high bubble concentration was observed along either sides of the bed close to the walls near the distributor, which gradually migrated inwards, spreading over the centre of the bed and higher up in it. A region of bubble deprivation was observed in the bed centre near the bottom. The tapering of bubble distribu-

* Corresponding author. Tel.: +44 1214144705; fax: +44 1214144719.
E-mail address: X.Fan@bham.ac.uk (X. Fan).

1385-8947/$ – see front matter © 2007 Elsevier B.V. All rights reserved.
doi:10.1016/j.cej.2007.10.013

Nomenclature

A_0	distributor plate area per hole (m^2)
A_t	cross-sectional area of the bed (m^2)
A_r	Archimedes number, $\rho_g(\rho_p - \rho_g)d_p^3 g/\mu_g^2$
d_B	spherical equivalent diameter of the bubble (m)
d_p	average size of solids (m)
D	diameter of a fluidised bed (m)
f_w	ratio of wake to the bubble by volume, $f_w = V_w/V_b$
g	gravitational acceleration (m/s^2)
h	height of the bubble above the distributor (m)
U	superficial gas velocity through a bed of solids (m/s)
U_B	velocity of a bubble rising through a bed (m/s)
U_{mf}	minimum fluidisation velocity (m/s)
V_x, V_y and V_z	particle velocities in x, y and z coordinates (m/s)
V_w	particle upward velocity in bubble and its wake (m/s)

Greek symbols

γ	the through flow factor
ρ_g, ρ_p	the densities for air and solid particles (kg/m^3)
μ_g	air viscosity (1.82×10^{-5} kg/ms)

tion also left the regions close to the wall in the upper part of the bed deprived of bubbles.

To predict the average rise velocity and average size of bubbles in a fluidised bed, many empirical correlations have been proposed [10,13–24], and several techniques have been developed to measure the physical properties of bubbles in fluidised beds, such as X-ray, ultra-fast magnetic resonance imaging [25–30]. In this study, attempts have been made to measure and characterise the bubbling pattern, average bubble size and its rise velocity through the analysis of the solid motion by using the positron emission particle tracking (PEPT) technique. The relationship between solid flow structure and the physical properties of bubbles is further discussed, and the comparison of PEPT measurement with empirical predictions is also reported.

2. Experimental technique and materials

The experimental setup consisted of a positron emission particle tracking system and a gas–solid fluidised bed as shown in Fig. 1. The gas–solid fluidised bed was a Plexiglas cylindrical column with 152 mm inner diameter and 1000 mm height. The column was placed vertically between the two γ-ray detectors of the Birmingham positron camera which cover a field of approximately 590 mm × 470 mm and offer a resolution of 1–2 mm under the conditions of this study. Air at ambient temperature was injected into the bed through a conical section, passing through a stainless steel porous plate distributor that supported the bed. The air was supplied by a GA11CFF air compressor and the flowrate was measured and controlled with calibrated rotameters.

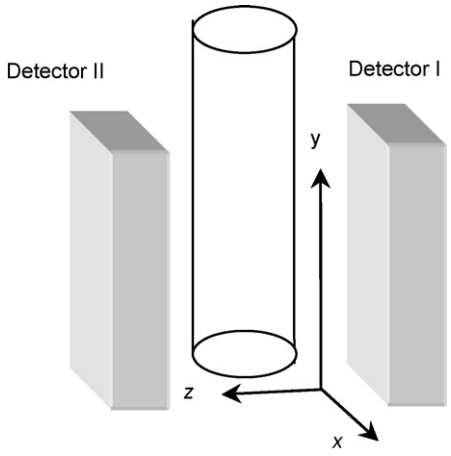

Fig. 1. Schematic diagram of the experimental setup.

The solids used were glass beads and polyethylene particles. A single polyethylene particle and a glass bead were radioactively labelled. Polyethylene is a less dense material (0.76 g/cm^3) and has a mean size of 717 μm. Glass is a dense material (2.7 g/cm^3) and has a mean size of 352 μm. Fig. 2 shows the size distribution of the polyethylene particles and glass beads. Both of them can be classified as group B according to the Geldart classification of particles [22]. Their Archimedes number, A_r, is 10,012 (polyethylene) and 4265 (glass beads). The initial bed height for both materials was approximately 152 mm, chosen to be equal to the bed diameter which would eliminate slugging [17]. All experiments were carried out in the bubbling regime which was characterised by the bed pressure drop and visual observation. The bed pressure drop was measured with a FC0510 micro-manometer interfaced to a PC through a RS232 port. To avoid disturbing the flow patterns, the bed pressure drop was measured after each PEPT measurement. The minimum fluidizing velocity U_{mf} was determined to be 0.24 m/s for the polyethylene bed and 0.15 m/s for the glass beads bed. For polyethylene, the fluctuation of the average pressure drop was not significant when the gas velocity increased from 0.24 to 1 m/s, and therefore, the fluidisation within this range can be

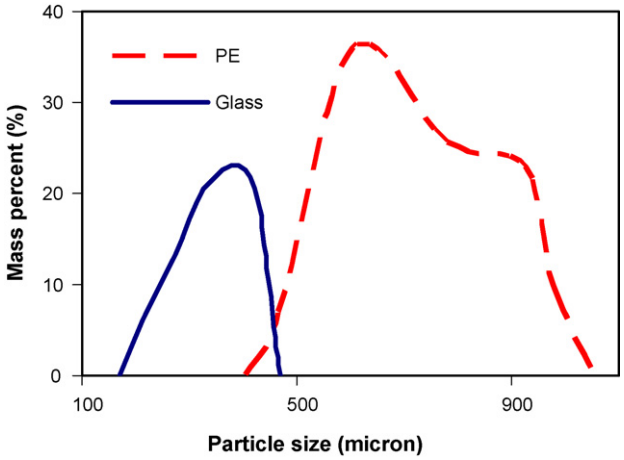

Fig. 2. Size distribution for the polyethylene particles and the glass beads.

seen to be in the bubbling regime [22,31]. Similarly for the glass beads, bubbling fluidisation can be achieved with gas velocities ranging from 0.15 to 0.7 m/s.

The tracking time for each experiment was 2 h and each experiment was repeated three times. Average results are presented hereafter. The obtained data, i.e., an extensive list of consecutive particle locations (every 4 ms), determine the instantaneous velocity as well as the probability of the tracer being located in specific parts of the equipment domain allowing an average velocity vector plot and an occupancy plot to be derived.

3. Particle tracking technique

Positron emission particle tracking (PEPT) technique consists of tracer labelling, detection of 511 keV gamma rays, and algorithms for location calculation and time reconstruction at every tracking step. When a polyethylene particle or a glass bead is labelled using ^{18}F, positrons annihilate with local electrons, resulting in emission of many γ-rays from the labelled particles. These γ-rays are in pairs and each pair emits almost exactly back-to-back, thus all γ-ray trajectories from the labelled particle can be triangulated back to (within the resolution of the camera) a point where the labelled particle is located. The location algorithm operates through minimizing the sum of perpendicular distances to the various trajectories of the γ-rays. To smooth the tracking, the γ-ray events detected within 1 s are usually divided into many sets. For a given set of events, the point that minimises the sum of perpendicular distances to the trajectories will be close to the tracer. The trajectories passing further away from the tracer are regarded as corrupted events and discarded. The minimum-distance point is recalculated using the remaining subset. The iteration procedure continues until the location of the tracer is calculated using just the uncorrupted events from the tracer [32–34].

For a selected set, S, of sequential trajectories, $L_1 \ldots L_N$, which are recorded as data from the camera, the sum of distances from any point (x, y, z) to the γ-ray trajectories can be stated as follows:

$$D_s(x, y, z) = \sum_s \delta_i(x, y, z) \tag{1}$$

where $\delta_i(x, y, z)$ is the distance of the ith trajectory from the point (x, y, z).

The minimum solution can be obtained by:

$$\frac{\partial D_s(x, y, z)}{\partial x} = 0, \quad \frac{\partial D_s(x, y, z)}{\partial y} = 0, \quad \frac{\partial D_s(x, y, z)}{\partial z} = 0 \tag{2}$$

The minimum distance point (x_0, y_0, z_0) is then obtained as the first approximation for the tracer position. The mean deviation of these trajectories from the minimum distance point is given by:

$$d_s(x_0, y_0, z_0) = \frac{D_s(x_0, y_0, z_0)}{N(S)} \tag{3}$$

where $N(S)$ is the number of events in the set S.

For a given set of trajectories, the first approximation (x_0, y_0, z_0) of the tracer is located using Eqs. (1) and (2), and the corresponding distance $\delta_i(x_0, y_0, z_0)$ of the ith trajectory to the point (x_0, y_0, z_0) is calculated. If the calculated $\delta_i(x_0, y_0, z_0)$ is larger than $kd_S(x_0, y_0, z_0)$, the trajectory is discarded, leaving a new subset S_1, in which the number of corrupted events is smaller. An improved location (x_1, y_1, z_1) with a small mean deviation $d_{S1}(x_1, y_1, z_1)$ is then calculated from this subset S_1 of events. The algorithm proceeds by iteration in this way, selecting subsets S_2, S_3, S_4, etc. The k in $kd_S(x_0, y_0, z_0)$ is a fixed parameter and determines the rate at which trajectories are discarded. The optimum value of the k lies somewhere between 1 and 1.5.

The final outcome is that the subset S_F of trajectories is selected from the original set, from which the location of particle, during the time interval covered by this subset, is calculated as its minimum distance point (x_F, y_F, z_F). Each event L_i has its time of measurement t_i recorded, and the location thus arrived at is considered to represent the particle's position at time

$$t = \frac{1}{N_F} \sum_{S_F} t_i \tag{4}$$

where $N_F \equiv N(S_F)$ is the number of trajectories in the final subset S_F.

Having located the particle once, the new set starts immediately from the end of the previous set. Despite being discarded as corrupt, during one iteration of the algorithm, many events actually correspond to later particle positions, and are thus involved in subsequent sets.

The final data will provide the tracer locations against the time in three dimensions (x, y, z). Typically, a radioactively labelled tracer can be located 100–200 times per second. In the past, this technique has been extensively used for characterisation of the solid motions [27,32–36].

The velocity of a tracer $\boldsymbol{v}_i = (v_{x_i}, v_{y_i}, v_{z_i})$ during the time interval between locations (x_i, y_i, z_i, t_i) and $(x_{i+1}, y_{i+1}, z_{i+1}, t_{i+1})$ is given by $v_{x_i} = (x_{i+1} - x_i)/(t_{i+1} - t_i)$, etc.

The tracer velocity is given by $v_{x_i} = (x_{i+1} - x_i)/(t_{i+1} - t_i)$, etc.

The tracer speed is given by $v = \sqrt{v_{x_i}^2 + v_{y_i}^2 + v_{z_i}^2}$.

4. Bubble size and rise velocity

4.1. Calculations of bubble velocity and bubble size by using the PEPT data

Several methods have been developed for the measurement of sizes and rise velocities of bubbles in fluidised beds. Many early measurements relied on submersible probe designs employing visible light or laser beam in 2-D beds to determine structure. X-ray and ultra-fast magnetic resonance imaging were developed later and used to study the rise velocities of bubbles non-intrusively in 3-D fluidising beds made of opaque materials [11,21,24,37].

In this study, the average rise velocities and sizes of bubbles in a fluidised bed are measured by using the data acquired by

Table 1
Correlations used most frequently for the prediction of bubble rise velocity

Davies and Taylor [13,14]	$U_B = 0.71 \times \sqrt{gd_B}$	For an isolated bubble
Davison and Harrison [15]	$U_B = U - U_{mf} + 0.711\sqrt{gd_B}$	Simple two-phase theory
Werther [20]	$U_B = (U - U_{mf}) + \phi(gd_B)^{0.5}$	For Geldart B particles, $\phi = 1.6D^{0.4}$, 0.1 m < D < 1 m
Wallis [16]	$U_B = 0.71 \times \sqrt{gd_B} \times 1.13\exp\left(-\frac{d_B}{D}\right)$ for $0.125 < \frac{d_B}{D} < 0.6$	For $0.125 < \frac{d_B}{D} < 0.6$
Kunii and Levenspiel [22]	$U_B = 1.6[(U - U_{mf}) + 1.13d_B^{0.5}]D^{1.35} + 0.711(gd_B)^{0.5}$	For Geldart B solids $D \leq 1$ m and $\frac{d_B}{D} < 0.125$
Baeyens and Geldart [17]	$U_B = \gamma(U - U_{mf}) + 0.711(gd_B)^{0.5}$	$\gamma = \frac{2.27}{A_r^{0.2}}$ $A_r = \frac{d_p^3\rho_g(\rho_p - \rho_g)g}{\mu_g^2}$

Where U_B is the average velocity of a bubble rising through a bed (m/s); d_B the spherical equivalent diameter of the bubble (m); U the superficial gas velocity through a bed of solids (m/s); U_{mf} the minimum fluidisation velocity (m/s); D the diameter of a fluidised bed (m); γ the through flow factor; A_r the Archimedes number; ρ_g and ρ_p are the densities for air and solid particles; d_p the average size of solids and μ_g is air viscosity [38], (1.82×10^{-5} kg/ms).

the non-intrusive PEPT technique. This is based on the fact that particle in bubble wakes or in bubbles travels upwards at an average velocity as high as the bubble. As illustrated by a number of studies, when a bubble travels upward through a bed of particles, the particles tend to flow around it in a manner somewhat like that encountered when a body moves through a fluid stream. Typical bubbles are not spherical but have a flattish profile. The region just below the bubble is the wake region. The particles in a wake and a bubble are carried along with the bubble as if attached to it for a certain distance [22,38]. Even though they are moving within the limited space, the average upward velocity of the particles in a wake and a bubble should be equal to the bubble rise velocity. The wake fraction, defined as the ratio of wake to the bubble by volume $f_w = V_w/V_b$, varies with bed materials, and is greater than 0.4 in most cases. For example, the f_w is greater than 0.4 for glass spheres, and is greater than 0.6 for acrylic granules [22]. There is also 0.2–1.0% of solids by volume in the bubbles. In considering the total volume of bubbles in a fluidised bed, the amount of solids in the wake is significant and large enough for the calculation of bubble rise velocity.

The velocity associated with particles in a bubble wake or in a bubble can be calculated by taking a suitable top fraction from the solid upward velocity map as shown in Figs. 4–6, since the upward velocities of particles in bubble wakes and in bubbles are significantly higher than those of the particles outside the wake and the bubble. The size of the top fraction can be determined from Fig. 3 which shows no significant difference in the rise velocity when the size is between 2 and 20%. This indicates that the top 10% of the upward velocity is certainly associated with the particles in the bubble and its wake. In order to see the bubble velocity at different bed levels, we divided the bed into a number of layers, and each layer being 5 mm in height. The average upward velocity of particles within the top 10% was calculated to represent the bubble rise velocity in each layer. These results will be presented later.

4.2. Prediction of bubble velocity and bubble size by using the empirical correlations

A number of correlations have been proposed to predict the average rise velocity and the average size of bubbles in fluidised beds. Table 1 shows the correlations used most frequently for the

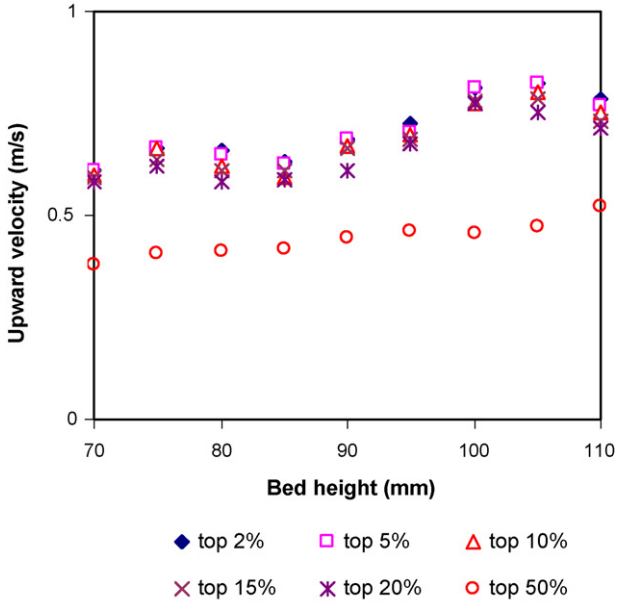

Fig. 3. Average rise velocities of particles as a function of the top fraction of the upward velocity map (V_y).

Table 2
Correlations used most frequently for the prediction of bubble size

Yasui and Johanson [14]	$d_B = 1.6\rho_p d_p\left(\frac{U}{U_{mf}-1}\right)^{0.63}h$
Whitehead and Young [21]	$d_B = 0.34\left(\frac{U}{U_{mf}-1}\right)^{0.33}h^{0.54}$
Rowe [19]	$d_B = \frac{(U-U_{mf})^{0.5}(h-h_0)^{3/4}}{g^{0.25}}$, $h_0 = 1.61[A_0{}^{1.6}g^{0.2}(U - U_{mf})^{-0.4}]^{1/3}$
Darton [10,39]	$d_B = 0.74(U - U_{mf})^{2/5}[h + 3.94\sqrt{A_0}]^{4/5}/g^{1/5}$
Werther [20]	$d_B = 8.53 \times 10^{-3}[1 + 27.2(U - U_{mf})]^{1/3}\cdot[1 + 6.84(h + h_0 - h_y)]^{1.21}$ for Geldart B type solids $h_0 - h_y \approx 0$
Mori and Wen [18]	$d_B = 0.652[A_t(U - U_{mf})]^{0.4} - \{0.652[A_t(U - U_{mf})]^{0.4} - 0.347[A_0(U - U_{mf}]^{0.4}\}\exp\left(\frac{-0.3h}{D_t}\right)$
Cai et al. [23]	$d_B = 0.21h^{0.8}(U - U_{mf})^{0.42} \times \exp[-0.25(U - U_{mf})^2 - 0.1(U - U_{mf})]$

prediction of bubble rise velocity proposed by Davies and Taylor (1950) [13,14]; Davison and Harrison (1963) [15]; Wallis (1969) [16]; Baeyens and Geldart (1974) [17]; Werther (1980) [20] and Kunii and Levenspiel (1991) [22]. Table 2 shows the correlations used most frequently for the prediction of bubble size proposed by Yasui and Johanson [14]; Whitehead and Young [21]; Rowe [19], Darton et al. [10,39]; Werther [20]; Mori and Wen [18] and Cai et al. [23].

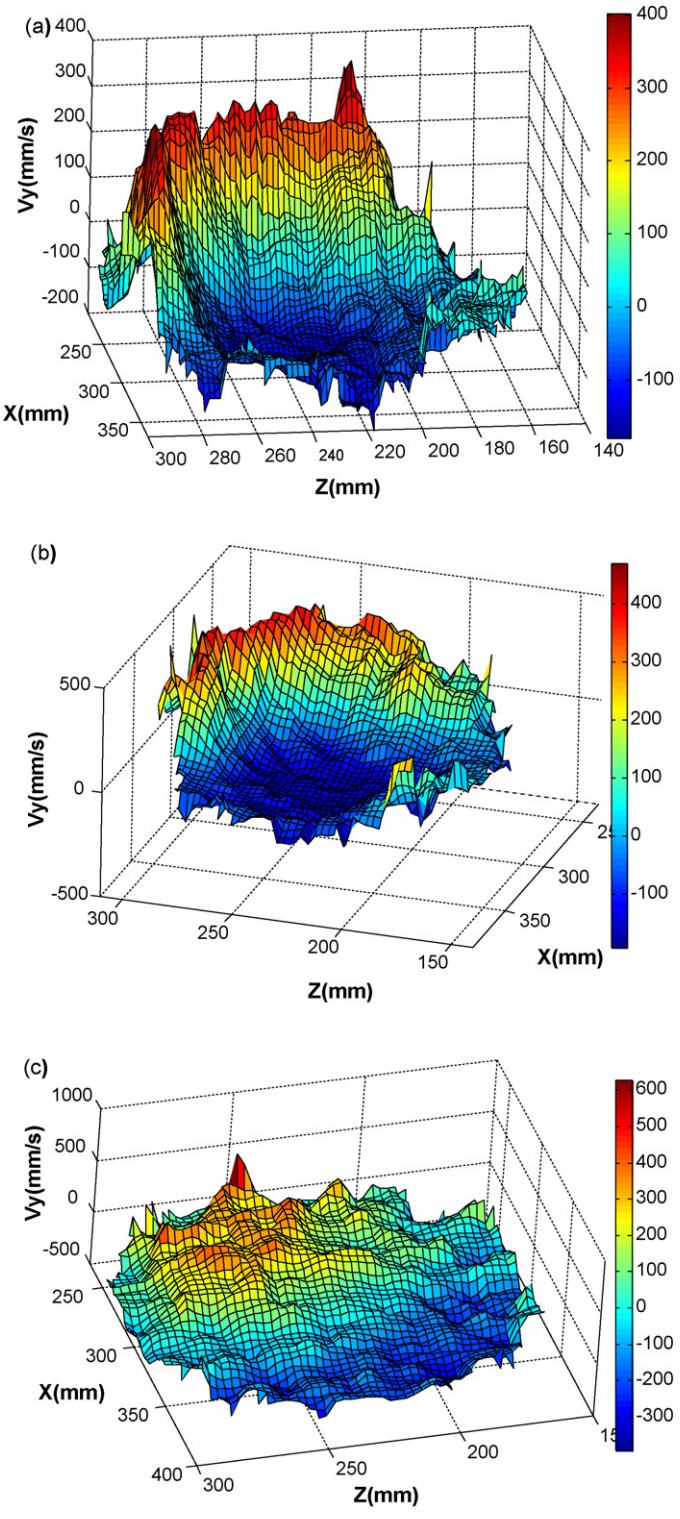

Fig. 4. Flow pattern A, bed material: glass beads, gas velocity $U - U_{mf} = 0.25$ m/s. (a) V_y at a bed height of 20 mm ($y = 160$ mm). (b) V_y at a bed height of 60 mm ($y = 200$ mm). (c) V_y at a bed height of 200 mm ($y = 340$ mm). (d) Solid flow pattern.

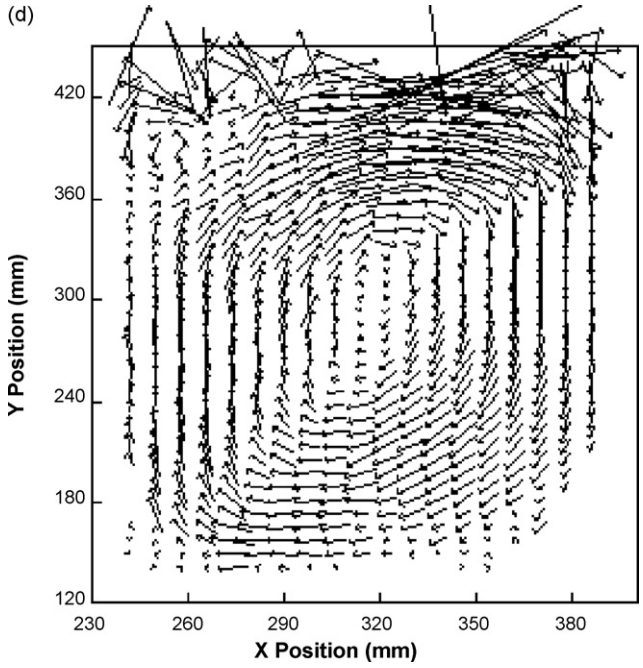

Fig. 4. (*Continued*)

5. Results and discussion

5.1. Solid flow patterns

A literature search shows that solid flow patterns in bubbling fluidised beds vary mainly with the bed height [22,40]. When the ratio of the bed height to the bed diameter is unity, the solid travels upwards either along the annulus or along the central part of the bed, inducing two circulation cells within the whole bed. However, the observation through PEPT measurements shows that solid flow pattern can vary significantly with the bed materials and gas velocity. Three types of flow patterns, designated patterns A, B and C, have been observed in our studies on glass beads and polyethylene fluidised beds as shown in Figs. 4–6, where the ratio of the bed height to the bed diameter is unity, and the superficial gas velocity was from 0.16 to 0.66 m/s. In the pattern A (Fig. 4), a single large circulation cell is observed within the whole bed, and particles move upwards at one side of the bed to the splash zone, and then return to the bed bottom along another side of the bed. This pattern can be observed in both glass beads and polyethylene fluidised beds when they are operated at a low superficial gas velocity ($U - U_{mf} < 0.25$ m/s for glass beads, $U - U_{mf} < 0.2$ m/s for polyethylene). It may not be a desirable flow pattern, but it reflects the effect of superficial gas velocity on solid/bubble flow structure.

Pattern B (Fig. 5) is a more typical flow pattern and has been reported frequently in literature. In a layer of 30 mm immediately above the air distributor, particles move upwards across

the whole area of the air distributor at a relative uniform velocity. After this layer, solids move inwards and travel upwards in the centre of the bed along the axis to the splash zone, and then return to the bed bottom along the annulus. The pattern reported in this study is observed in a glass beads fluidised bed when it is operated at a superficial gas velocity ($U - U_{mf}$) of 0.42 m/s.

The pattern C (Fig. 6) is observed in this study through the PEPT technique when a polyethylene fluidised bed is operated at a superficial gas velocity ($U - U_{mf}$) of 0.25–0.50 m/s, and the ratio of bed height to the bed diameter is unity. Solid motion in the pattern C is much more complex than that observed in patterns A and B. The bed can be divided into three sections. At the bottom section, solids travel upwards along the annulus, and move down in the bed centre. At the top section, solids travel upwards at the centre of the bed along the axis to the splash zone and then return to the intermediate height of the bed along the annulus. At the intermediate height of the bed (60–100 mm), the upward solid flow from the bottom section encounters the downward flow from the top section of the bed at the annulus (Fig. 6d). The two solid flows merge and change the direction towards the bed centre where the particles are mixed and redistributed to the circulation cells at bottom and top sections. A similar flow pattern is also observed in sand (90 μm) fluidised beds with bed diameters of 150 mm and 90 mm in our studies.

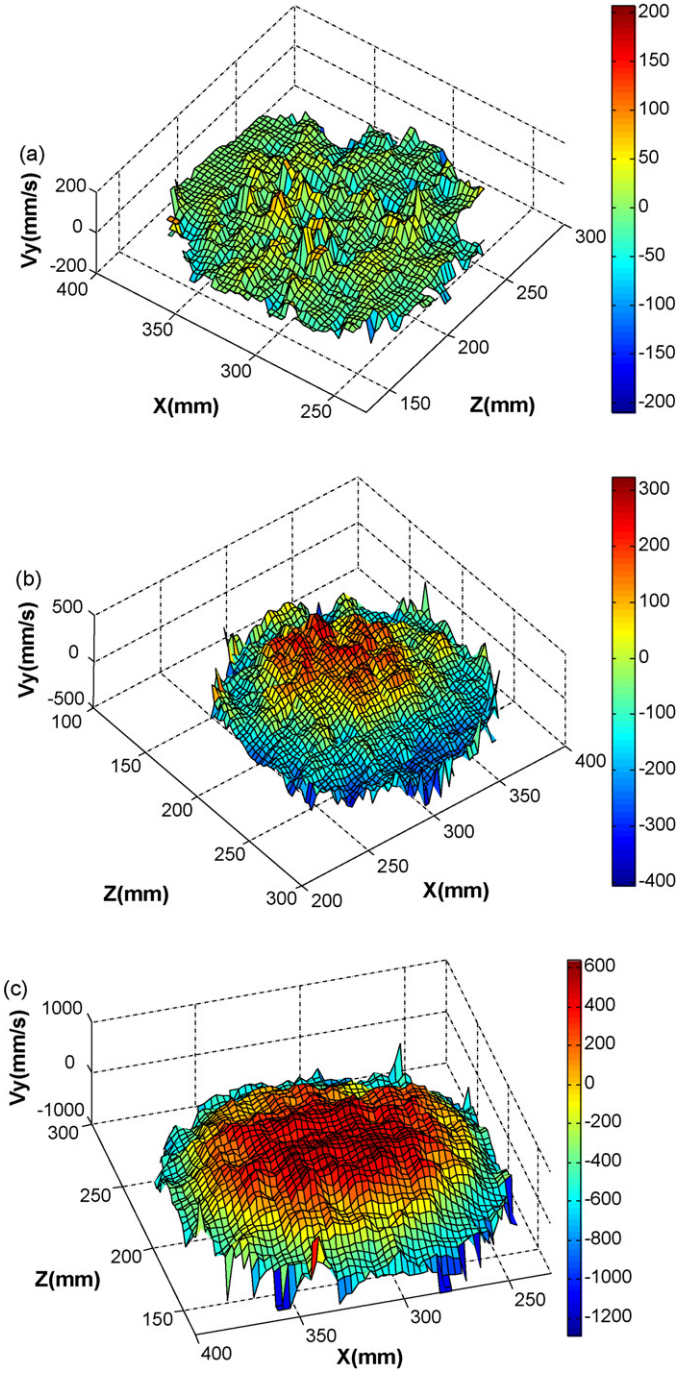

Fig. 5. Flow pattern B, bed material: glass beads, gas velocity $U - U_{mf} = 0.42$ m/s. (a) V_y at a bed height of 20 mm ($y = 160$ mm). (b) V_y at a bed height of 60 mm ($y = 200$ mm). (c) V_y at a bed height of 160 mm ($y = 300$ mm). (d) Solid flow pattern.

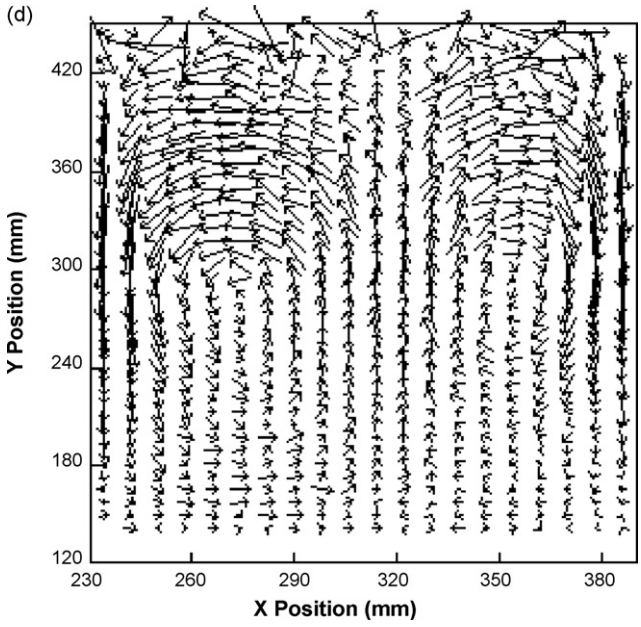

Fig. 5. (*Continued*)

5.2. Bubble flow patterns

The bubble flow patterns in the studied fluidised beds can be disclosed through analysing the solid flow structure and the solid upward velocity map. As described earlier, the solids in a fluidised bed are driven upwards by air bubbles. The upward velocity (V_y) of solids is higher in the bubbles or their wakes than in the region away from the bubble path. The peaks of the V_y map of solids, therefore, correspond to the position of bubbles. Through plotting the V_y map at any level of the bed, the favoured ascending gas channels can be identified through the cumulative acquisition of large quantities of data during PEPT measurements.

Figs. 4–6 show the solids V_y map for the conditions under which the three solid flow patterns can be observed, where each experiment was lasted for 2-h. It can be seen that the favoured ascending gas channels vary greatly with bed materials and

superficial gas velocity. Three patterns of bubble flows, corresponding to the three solid flow structures, have been observed in this study. In pattern A, the favoured channel of ascending bubbles was located at one side of the bed under the experimental conditions. As shown in Fig. 4, there was not a single bubble that travelled upwards from the valley region within the 2-h experiment. The injected air was forced to one side of the bed by the returning flow of solids, inducing a large circulation cell within the whole bed. This pattern (A) was observed when the glass beads or polyethylene fluidised beds were operated at a low superficial gas velocity ($U = 0.40$ m/s for glass beads, 0.34 m/s for polyethylene particles).

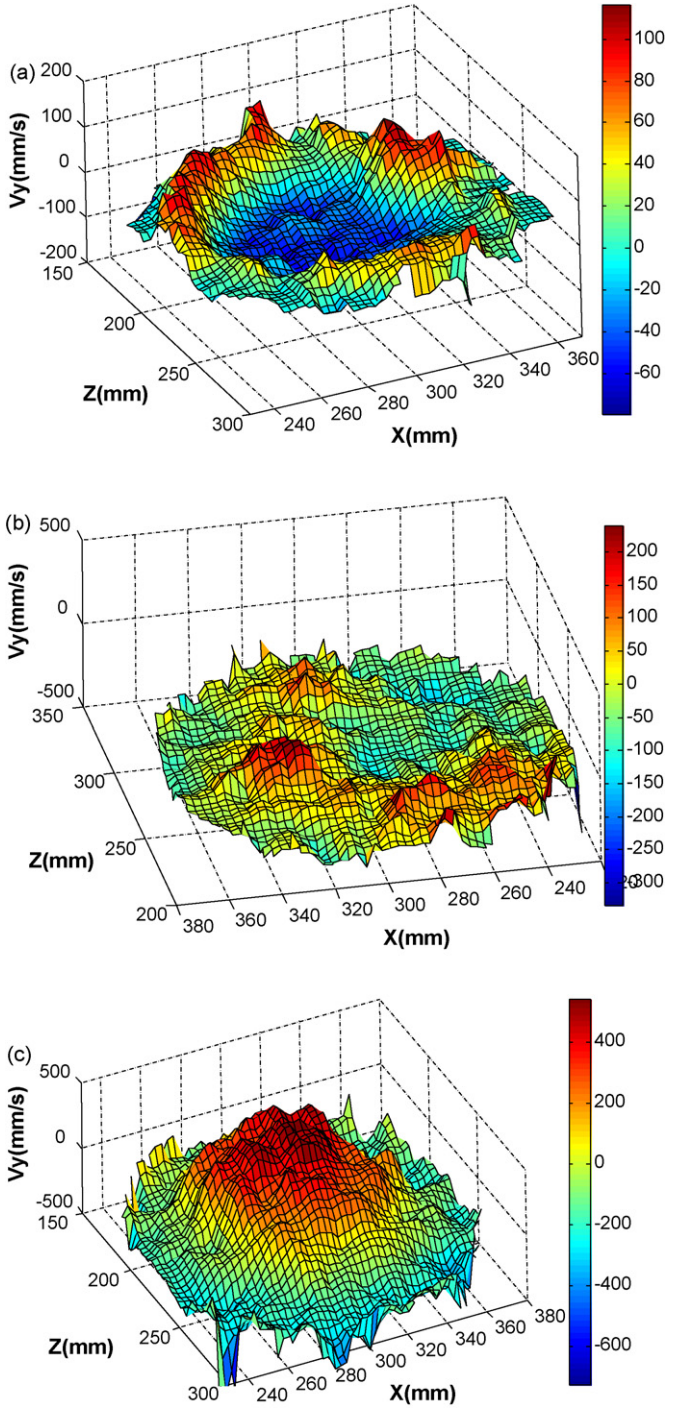

Fig. 6. Flow pattern C, bed material: polyethylene, gas velocity $U - U_{mf} = 0.25$ m/s. (a) V_y at a bed height of 20 mm ($y = 160$ mm). (b) V_y at a bed height of 90 mm ($y = 230$ mm). (c) V_y at a bed height of 210 mm ($y = 350$ mm). (d) Solid flow pattern.

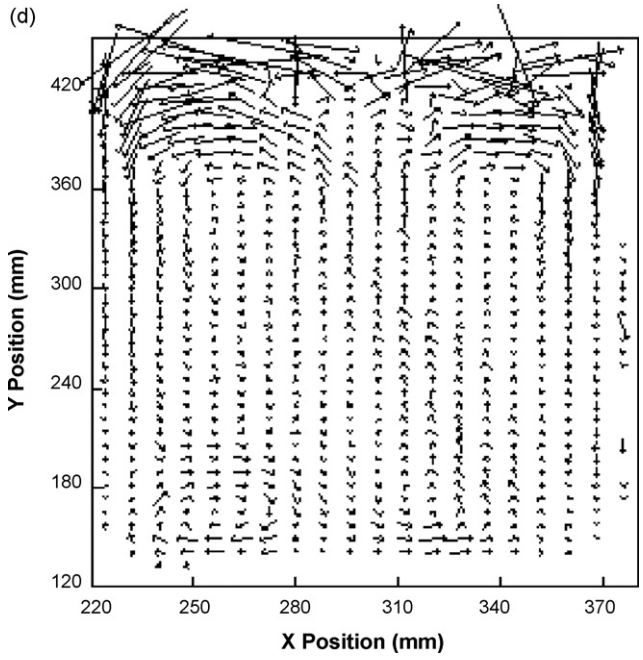

Fig. 6. (*Continued*)

Pattern B of the bubble flow (Fig. 5) was observed when the glass beads fluidised bed was operated at a superficial gas velocity ($U - U_{mf}$) of 0.42 m/s. The solid velocity V_y was relatively uniform within a 30 mm layer immediately above the air distributor (Fig. 5a), then a peak in the V_y map was observed in the central region of the bed (Fig. 5b). This indicates that the bubbles distributed relatively uniformly in a layer close to the distributor. The rising bubbles then moved inwards to the central region of the bed. This bubble flow pattern agrees with the observations from Grace and Harrison [9] and Darton et al. [10], where the air bubbles are relatively uniformly distributed in a layer close to the distributor and then coalesced and shafted inwards to the central region of the bed with the increase in the bed height, resulting in the emptying of bubbles in the region near the walls.

When the polyethylene fluidised bed was operated at superficial gas velocities ($U - U_{mf}$) of 0.25 and 0.42 m/s, the bubble flow followed the pattern C. Air bubbles were favoured to form and initially travel upwards in the annulus of the bed, rather than being uniformly distributed in the whole cross-section area. Fig. 6a shows that there was not a single air bubble that travelled upwards in the central region of the bed at the bottom section throughout the entire data collection period of 2 h. The bubbles then moved inwards to the central region at an intermediate height of the bed (60–100 mm) by the solid flows returning from the top section of the bed as shown in Fig. 6c and d. Above the intermediate layer, air bubbles travelled upwards from the central region of the bed and formed a peak in the V_y map as shown in Fig. 6c and d. This agrees with the bubble flow pattern observed by Werther and Molerus [11,12] and Lim et al. [8].

Overall, the favoured ascending gas channels within a bubbling fluidised bed varies not only with bed geometry and the ratio of bed height to bed diameter as described in literature [22,40], but also appears to vary with bed materials and superficial gas velocity. Under the similar operation conditions, different bed materials give a different gas/solid flow pattern.

5.3. Comparison of PEPT measurement with empirical predictions

Many empirical correlations have been proposed to predict the rise velocity and the size of bubbles in fluidised beds as listed in Tables 1 and 2. In this section, the investigation will focus on the comparison of the PEPT measurement with empirical predictions, and on the impact of gas/solid flow pattern on the rise velocity and the size of air bubbles.

Firstly, the bubble sizes are calculated by using equations listed in Table 2, respectively for each flow pattern (A, B and C). The calculated bubble sizes are then put into each correlation listed in Table 1 to calculate the bubble rise velocity. There are totally 42 combinations of velocity-size correlations, i.e., for each flow pattern, 42 calculated values can be obtained for the bubble rise velocity. Figs. 7–9 present those results that have a good agreement between the PEPT measurements and empirical predictions for the flow patterns A, B and C. For pattern A, the PEPT measurements agree well with the rise velocities calculated from Eqs. (5)–(7) and (9)–(10) as shown in Figs. 7–9. The equations are the combinations of Baeyens–Rowe, Baeyens–Yasui, Werther–Darton, Kunii–Rowe and Kunii–Yasui. The rise velocities calculated from the PEPT data agree well with Eqs. (5)–(10) for the flow pattern B, where the Eq. (8) is the combination of Davison and Darton.

For the flow pattern C, the bubble rise velocities calculated by using particle rise velocity in bubble wakes and in bubbles did not show a constant increase with the bed height as indicated by the empirical approaches. The bubble rise velocity firstly increased with the bed height to 0.7 m/s, and then decreased to 0.35 m/s at the bed height from 130 mm ($y = 270$) to 200 mm ($y = 340$). Above a bed height of 200 mm, the rise velocity dramatically increased again. This data matched very well with the measured solid flow structure. The empirical correlations listed in Eqs. (6) and (10)–(13) can be used to predict the bubble rise velocity at the bottom section of the bed ($h < 150$ mm) for the pattern C, but cannot predict the bubble rise velocity at the intermediate level of the bed. The explanation could be that the empirical correlations were deduced based on the flow patterns A or B (Figs. 4 and 5), rather than on the pattern C. In the pattern C, the air bubbles travel upward along the annulus in the bottom section of the bed, and then shifted to the bed centre in the intermediate section of the bed; therefore, the bubble sizes and bubble rise velocity are reduced. After the intermediate height of the bed, the bubbles rapidly coalesce again, resulting in a fast increase in the bubble size and their rise velocity. Another reason may be due to some empirical models used in the work for bubbles are

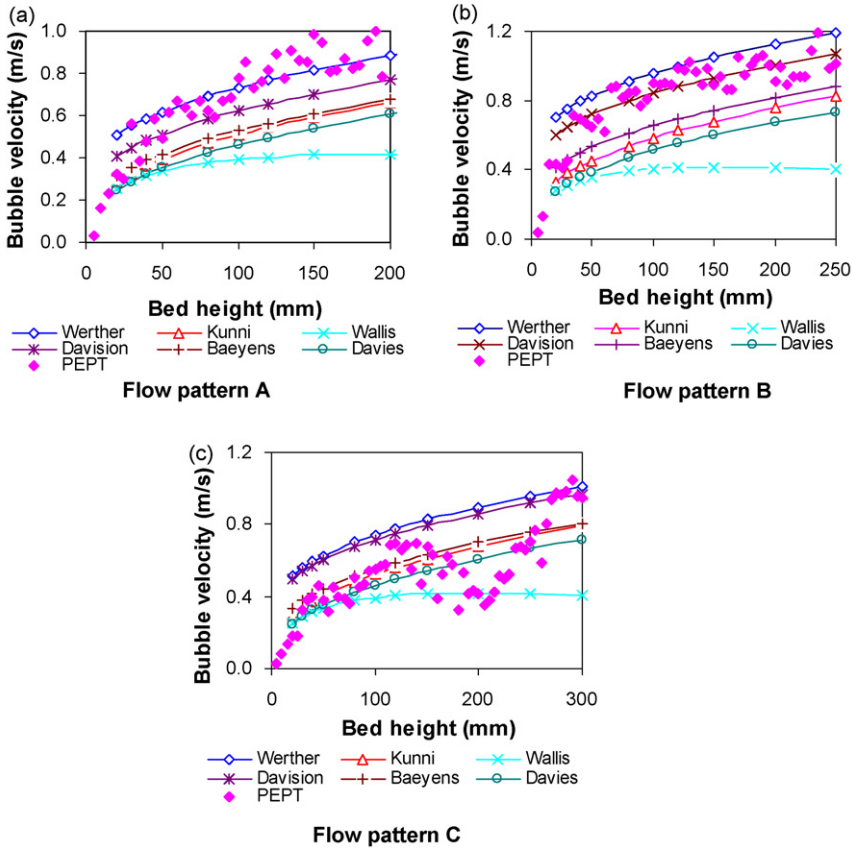

Fig. 7. Comparison of bubble velocity measured by PEPT with empirical correlations, where bubble sizes are calculated by using Darton correlations.

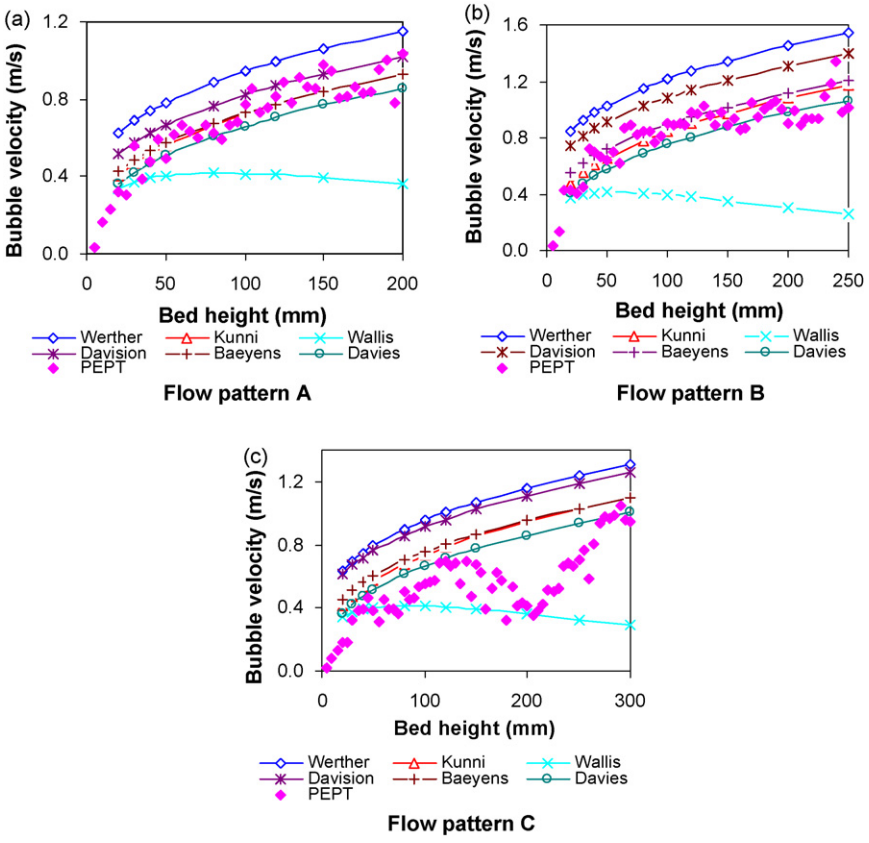

Fig. 8. Comparison of bubble velocity measured by PEPT with empirical correlations, where bubble sizes are calculated by using Rowe correlation.

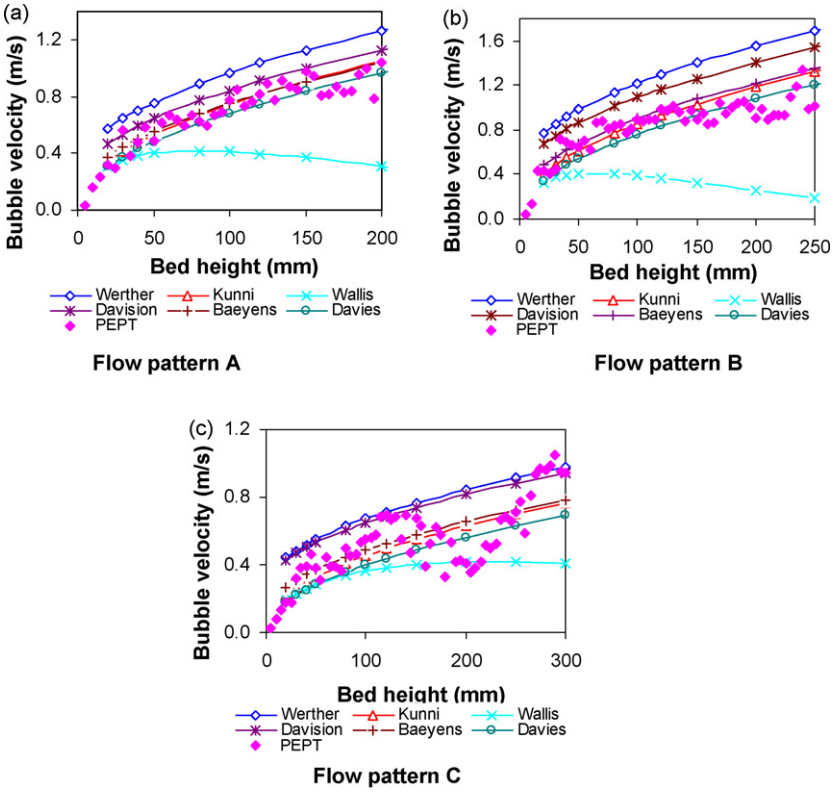

Fig. 9. Comparison of bubble velocity measured by PEPT with empirical correlations, where bubble sizes are calculated by using Yasui correlation.

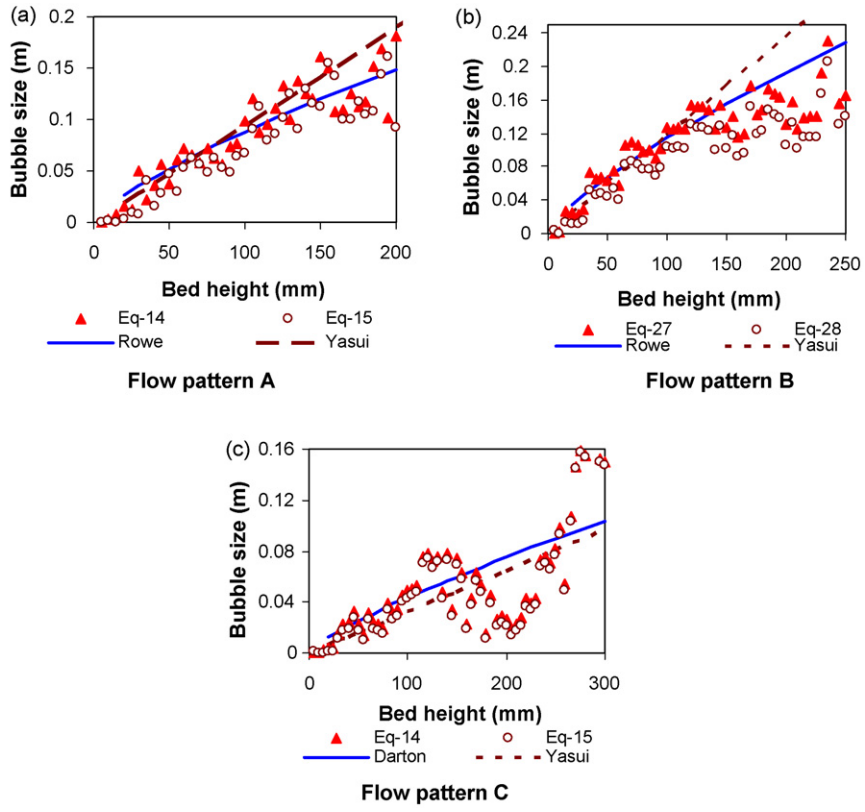

Fig. 10. Air bubble sizes calculated by using Eqs. (14) and (15), and empirical correlations from Darton, Rowe and Yasui.

two-dimensional, and agreement with fully three-dimensional measurements is difficult due to coalescence and splitting.

Combination of Baeyens–Rowe:

$$U_B = \frac{2.27}{A_r^{0.2}}(U - U_{mf}) + 0.711\sqrt{g^{0.75}(U - U_{mf})^{0.5}(h + h_0)^{0.75}} \quad (5)$$

with $h_0 = 1.61[A_D^{1.6} g^{0.2}(U - U_{mf})^{-0.4}]^{1/3}$

Combination of Baeyens–Yasui:

$$U_B = \frac{2.27}{A_r^{0.2}}(U - U_{mf}) + 0.711\sqrt{1.6 g \rho_P d_P \left(\frac{U}{U_{mf} - 1}\right)^{0.63} h} \quad (6)$$

Combination of Werther–Darton:

$$U_B = (U - U_{mf}) + 1.6D^{0.4}\sqrt{0.74 g^{0.8}(U - U_{mf})^{0.4}(h + 3.94A_0^{0.5})^{0.8}} \quad (7)$$

Combination of Davison and Darton:

$$U_B = (U - U_{mf}) + 0.611 g^{0.4}(U - U_{mf})^{0.2}(h + 3.94A_0^{0.5})^{0.4} \quad (8)$$

Combination of Kunii–Rowe:

$$U_B = 1.6D^{1.35}(U - U_{mf}) + (1.81D^{1.35} + 0.711g^{0.5})\sqrt{\frac{(U - U_{mf})^{0.5}(h - h_0)^{0.75}}{g^{0.25}}} \quad (9)$$

Combination of Kunii–Yasui:

$$U_B = 1.6D^{1.35}(U - U_{mf}) + (1.81D^{1.35} + 0.711g^{0.5})\sqrt{1.6\rho_p d_p \left(\frac{U}{U_{mf} - 1}\right)^{0.63} h} \quad (10)$$

Combination of Baeyens–Darton:

$$U_B = \frac{2.27}{A_r^{0.2}}(U - U_{mf}) + 0.611 g^{0.4}(U - U_{mf})^{0.2}(h + 3.94A_0^{0.5})^{0.4} \quad (11)$$

Combination of Kunii–Darton:

$$U_B = 1.6D^{1.35}(U - U_{mf}) + (1.81D^{1.35} + 0.711g^{0.5}) \frac{0.86(U - U_{mf})^{0.2}\left(h + 3.94\sqrt{A_0}\right)^{0.4}}{g^{0.1}} \quad (12)$$

Combination of Davies–Darton:

$$U_B = 0.611 g^{0.4}(U - U_{mf})^{0.2}(h + 3.94A_0^{0.5})^{0.4} \quad (13)$$

5.4. Prediction of bubble size by using solid upward velocity in bubble wakes

From the results listed in Figs. 7–9, it can be seen that the bubble rise velocities calculated from the PEPT measurement have a good agreement with many correlations, particularly with the correlations proposed by Baeyens and Kunii. Based on these two correlations, Eqs. (14) and (15) are derived for calculating the bubble size in the studied bubbling fluidised beds by using the upward velocity of particles in bubble wakes and in bubbles. From Fig. 10, it can be seen that the bubble size calculated from Eqs. (14) and (15) can reflect the variation of solid/bubble flow pattern. For the flow patterns A and B, the air bubbles travel straight upwards from the air distributor to the splash zone, and their sizes increased constantly when rising through the fluidised bed. The bubble sizes calculated by using the upward velocity of particles in bubbles and their wakes agree well with the predictions from Rowe (Eq. (13)) and Yasui (Eq. (11)). For the flow pattern C, the bubble size calculated by using the PEPT data is significantly different from the empirical prediction and the descriptions in literature. The bubble sizes firstly increase until the bed height of 150 mm ($y = 290$) and then reduce in the middle section of the bed, rather than expanding constantly. This matches the solid/bubble flow structure detected by the PEPT technique. The bubble size in the intermediate section of the bed is much smaller than the predictions from empirical correlations. Above the bed height of 200 mm ($y = 340$), the bubbles expand again rapidly, and the expanding rate is much higher than the predicted value.

$$d_B = \left(\frac{V_w - 1.6D^{1.35}(U + U_{mf})}{1.81D^{1.35} + 0.711g^{0.5}} \right)^2 \quad (14)$$

$$d_B = \frac{[V_w - \gamma(U + U_{mf})]^2}{0.506g} \quad (15)$$

where V_w is particle upward velocity in bubble and its wake (m/s),

$$\gamma = \frac{2.27}{A_r^{0.2}}, \quad A_r = \frac{d_p^3 \rho_g (\rho_p - \rho_g) g}{\mu_g^2}$$

6. Conclusions

It has been demonstrated that bubble flow pattern and the bubble behaviour are much more complex than the descriptions in literature when the beds are operated in a bubbling regime and the ratio of bed height to bed diameter is unity. They can vary greatly with the bed materials and applied gas velocity. Three types of patterns (A, B and C) have been observed in this study on the glass beads and polyethylene fluidised beds. For the pattern A, a favoured channel of ascending gas is found along one side of the bed when the glass beads bed and the polyethylene bed are operated at a low superficial gas velocity. It is not a favourable flow pattern for mixing and chemical reaction but reflects the effect of operating gas velocity on the bubble flow pattern. In this pattern (A), the bubbles travel straight upwards, their size and rise velocity increased constantly through the vertical plane. For the pattern B, the bubbles distribute relatively uniformly in a layer close to the distributor, and then move inwards to the central region of the bed. The size and rise velocity of the bubbles also increase constantly through the beds. Pattern C is a newly observed flow pattern and manifests itself when the polyethylene fluidised bed is operated at superficial gas velocity ($U - U_{mf}$) of 0.25–0.5 m/s and the ratio of bed height to bed diameter is unity. In this pattern, air bubbles are favoured to form and initially travel upwards in the annulus of the bed, rather than uniformly distribute in the whole cross-section area. The bubbles are splitting and move inwards to the central region at an intermediate height of the bed by the solid flows returning from the top section of the bed. Above the intermediate layer, air bubbles travel upwards from the central region of the bed and expand rapidly. The bubble size and rise velocity do not increase constantly as described in the literature. The rise velocity firstly increased with the bed height to 0.7 m/s, and then decreased to 0.35 m/s at the intermediate level of the bed. At the top section of the bed, the rise velocity and bubble size dramatically increased again.

The comparison of the results calculated by using upward velocity of solids in bubbles and their wakes with the predictions from a number of empirical correlations indicates that non-intrusive positron emission particle tracking (PEPT) can be a potential technique for measuring the bubble size and bubble rise velocity. The bubble rise velocity is calculated based on the solid upward velocity in bubbles and their wakes, and the bubble size in this study is calculated by using the Eqs. (14) and (15).

References

[1] A.D. Salman, M.J. Hounslow, Fluidized bed applications, Chem. Eng. Sci. 62 (1–2) (2007) 1.
[2] Y. He, H. Lu, Q. Sun, L. Yang, Y. Zhao, D. Gidaspow, J. Bouillard, Hydrodynamics of gas–solid flow around immersed tubes in bubbling fluidized beds, Powder Technol. 145 (2004) 88–105.
[3] G.A. Bokkers, M. van Sint Annaland, J.A.M. Kuipers, Mixing and segregation in a bidisperse gas–solid fluidised bed: a numerical and experimental study, Powder Technol. 140 (2004) 176–186.
[4] R. Clift, J.P.K. Seville, Gas Cleaning at High Temperatures, Blackie Academic & Professional, London, 1993.
[5] K. Shibata, M. Shimizu, S. Inaba, R. Takahashi, J. Yagi, Pressure loss and hold-up powders for gas-powder two-phase flow in packed beds, ISIJ Int. 31 (1991) 34–439.
[6] M.C. Leaper, J.P.K. Seville, N. Hilal, S.W. Kingman, A.S. Burbidge, Investigating the dynamics of segregation of high jetsam binary batch fluidised bed systems, Chem. Eng. Proc. 43 (2004) 187–192.
[7] C.N. Lim, M.A. Gilbertson, A.J.L. Harrison, Measurement and simulation of bubbling fluidised beds, Powder Technol. 170 (2006) 67–177.
[8] C.N. Lim, M.A. Gilbertson, A.J.L. Harrison, Bubble distribution and behaviour in bubbling fluidised beds, Chem. Eng. Sci. 62 (2007) 56–69.
[9] J.R. Grace, D. Harrison, The distribution of bubbles within a gas-fluidized bed, Inst. Chem. Eng. Symp. Ser. 30 (1969) 105–125.
[10] R.C. Darton, R.D. LaNauze, J.F. Davidson, D. Harrison, Bubble growth due to coalescence in fluidised beds, Trans. Inst. Chem. Eng. 55 (1977) 274–280.
[11] J. Werther, O. Molerus, The local structure of gas fluidized beds-I. A statistically based measuring system, Int. J. Multiphase Flow 1 (1973) 103–122.
[12] J. Werther, O. Molerus, The local structure of gas fluidized beds-II. The spatial distribution of bubbles, Int. J. Multiphase Flow 1 (1973) 103–122.

[13] R.M. Davies, G.I. Taylor, The mechanics of large bubbles rising through extended liquids and through liquids in tubes, in: Proceedings of the Royal Society of London, Series A, Mathemat. Phys. Sci. 200 (1950) 375–390.
[14] G. Yasui, L.N. Johanson, Characteristics of gas pockets in fluidized beds, AIChE J. 4 (4) (1958) 445–452.
[15] J.F. Davidson, D. Harrison, Fluidized Particles, Cambridge University Press, New York, 1963.
[16] G.B. Wallis, One-dimensional Two-Phase Flow, McGraw-Hill, New York, 1969.
[17] J. Baeyens, D. Geldart, An investigation into slugging fluidized beds, Chem. Eng. Sci. 29 (1974) 255–265.
[18] C. Mori, C.Y. Wen, Estimation of bubble diameter in gaseous fluidized beds, AIChE J. 21 (1975) 109–115.
[19] P.N. Rowe, Prediction of bubble size in a gas fluidised bed, Chem. Eng. Sci. 31 (1976) 285–288.
[20] J. Werther, Hydrodynamics and mass transfer between the bubble and emulsion phases in fluidized beds of sand and cracking catalyst, in: D. Kunii, R. Toei (Eds.), Fluidization, Engineering Foundation, New York, 1983.
[21] A.B. Whitehead, A.D. Young, Fluidization performance in large scale equipment: Part I, in: Proc. Intern. Symp. on Fluidization, Eindhoven, Netherlands, 1967, p. 284.
[22] D. Kunii, O. Levenspiel, Fluidization Engineering, second ed., Butterworth-Heinemann, Boston, 1991.
[23] P. Cai, M. Schiavetti, G. De Michele, G.C. Grazzini, M. Miccio, Quantitative estimation of bubble size in PFBC, Powder Techol. 80 (1994) 99–109.
[24] C.R. Müller, J.F. Davidson, J.S. Dennis, P.S. Fennell, L.F. Gladden, A.N. Hayhurst, M.D. Mantle, A.C. Rees, A.J. Sederman, Rise velocities of bubbles and slugs in gas-fluidised beds: ultra-fast magnetic resonance imaging, Chem. Eng. Sci. 62 (2007) 82–93.
[25] J.Z. Xue, E. Herbolzheimer, M.A. Rutgers, W.B. Russel, P.M. Chaikin, Diffusion, dispersion, and settling of hard spheres, Phys. Rev. Lett. 69 (1992) 11–14.
[26] R. Wang, M.S. Rosen, D. Candela, R.W. Mair, R.L. Walsworth, Study of gas-fluidization dynamics with laser-polarized ^{129}Xe, Magn. Reson. Imag. 23 (2005) 203–207.
[27] Y.L. Ding, Z. Wang, D. Wen, M. Ghadiri, X. Fan, D. Parker, Solids behaviour in a dilute gas–solid two-phase mixture flowing through monolith channels, Chem. Eng. Sci. 61 (2006) 1561–1570.
[28] S. Cooper, C.J. Coronella, CFD simulations of particle mixing in a binary fluidized bed, Powder Technol. 151 (2005) 27–36.
[29] J.P.K. Seville, C.D. Willett, P.C. Knight, Interparticle forces in fluidisation: a review, Powder Technol. 113 (2000) 261–268.
[30] R. Jackson, The Dynamics of Fluidized Particles, Cambridge University Press, Cambridge, 2000.
[31] K.D. Kafui, C. Thornton, M.J. Adams, Discrete particle-continuum fluid modelling of gas–solid fluidised beds, Chem. Eng. Sci. 57 (2002) 2395–2410.
[32] D.J. Parker, C.J. Broadbent, P. Fowles, M.R. Hawkesworth, P. Mcneil, Positron emission particle tracking—a technique for studying flow within engineering equipment, Nucl. Instr. Meth. A 326 (1993) 592–607.
[33] D.J. Parker, D.A. Allen, D.M. Benton, P. Fowles, P.A. McNeil, M. Tan, T.D. Beynon, Developments in particle tracking using the Birmingham positron camera, Nucl. Instr. Meth. A 292 (1997) 421–426.
[34] Z. Yang, D.J. Parker, P.J. Fryer, S. Bakalis, X. Fan, Multiple-particle tracking—an improvement for positron particle tracking, Nucl. Instr. Meth. A 564 (2006) 332–338.
[35] M. Stein, Y.L. Ding, J.P.K. Seville, D.J. Parker, Solids motion in bubbling gas fluidised beds, Chem. Eng. Sci. 55 (2000) 5291–5300.
[36] M. Stein, Y.L. Ding, J.P.K. Seville, Experimental verification of the scaling relationships for bubbling gas-fluidised beds using the PEPT technique, Chem. Eng. Sci. 57 (2002) 3649–3658.
[37] J.M. Burgess, P.H. Calderbank, The measurement of bubble parameters in two-phase dispersions—II: The structure of sieve tray froths, Chem. Eng. Sci. 30 (1975) 1107–1121.
[38] J.R. Howard, Fluidized Bed Technology: Principle and Applications, Adam Higer, Bristol and New York, 1989.
[39] Y.S. Wong, Particle motion in relatively thin fluidised bed models, Chem. Eng. Sci. 61 (2006) 6234–6238.
[40] G.R. Duursma, D.H. Glass, S.J.L. Rix, M.I. Yorquez-Ramirez, PIV investigations of flow structures in the fluidised bed freeboard region, Powder Technol. 120 (2001) 2–11.